 doi:10.20944/preprints202208.0319.v1

Determining Interannual Variability of the Annual Cycle

ZHANG Meng[1], Hans VON STORCH[*2]

[1] South China Sea Information Center, State Oceanic Administration, 510310, Guangzhou, China

[2]Institute of Coastal Systems, Hereon Research Centre, 21502, Geesthacht, Germany

Abstract

We present a method to study the interannual variability of the annual cycle. The method consists of first determining the amplitude and phase of segments of 12 monthly means at all spatial points, resulting in one complex number per grid point and per year. The complex fields, once per year, are then subject to a complex EOF (CEOF) analysis.

We consider as an example the barotropic stream function in the South China Sea as simulated with an ocean general circulation model across 6 decades of years, driven my realistic (NCEP) weather forcing. We find 3 to 4 to "significant" CEOFs, which account for about 53 to 62% of variance. These CEOFs go with large-scale patterns. Their time coefficients are mostly stationary, but point to some inhomogeneities related to instationarities in the forcing. In particular, the simulation since 1950-1958 deviates from the remainder of the simulation.

The first CEOF describes variations in the center of the South China Sea. Its principal component describes a systematic, albeit noisy shift by almost 180° from 1960 to about the year 2000. When overlaid the long-term mean annual mean, the overall change consists of an amplification of the annual cycle in the 1960s and 1990s, whereas In the 1970s, the amplitude was reduced. Phase shifts in the anomaly (given by the CEOFs) have a small effect, because of the dominance of the mean annual cycle. These variations are not related to ENSO variability but may origin in variations of the Southeast monsoon. The second EOF represents strong changes, both in terms of intensity and phase, in the Luzon strait.

Keywords: annual cyckle; complex EOFs; statistical analysis; South China Sea

1. Introduction

Usually, the strongest climate change signal of all, the annual cycle receives little attention. Indeed, as Stine et al. (2009) assert: "The annual cycle in the Earth's surface temperature is extremely large—comparable in magnitude to the glacial–interglacial cycles over most of the planet." This cycle is considered simple to predict, mostly considered trivially, but of utmost practical significance. It is related to the solar output and is thus a deterministically forced signal. As such it is by and large well simulated in climate models, which is – on the side – a perfect proof that climate models can describe robustly externally forced signals in the chaotic climate system.

Preprints (www.preprints.org) | NOT PEER-REVIEWED | Posted: 17 August 2022 doi:10.20944/preprints202208.0319.v1

In recent years, some attention has emerged with respect to the possibility of a change of the annual cycle related to Global Warming (Wallace and Osborn, 2002; Thomson, 2009; Dwyer et al., 2012; Marcel et al., 2017; Wainwright et al., 2021), but this is not the subject of the present article.

The annual cycle varies to some extent from year to year, reflecting the effect of stochastic weather variations or internal variability (e.g., van Loon et al., 1993; Tesouri et al., 2005 Stine et al., 2009; Stine and Huybers, 2012; Vecchio and Carbone, 2010; Deng et al., 2018; Zhang et al. , 2019). Many of these studies dealt with atmospheric dynamics, but there are also studies on regional oceanographic dynamics (Männikus et al., 2020).

Variations of the annual cycle, in particular of precipitation was studied by conventional EOFs, with a first one named "solstitial mode" and a second named "equinoctial asymmetric mode." (Wang and Ding, 2008; Ha et al., 2012). Here, we suggest a different method, based on first the harmonic analysis of each annual segment resulting in an amplitude/phase complex number at each grid point (as done by Wallace and Osborn, 2002, and Tesouri et al., 2005), followed by a complex EOF analysis (e.g., von Storch and Zwiers, 1999).

We briefly sketch the complex EOF analysis in Section 2, and introduce the example, namely annual variations of currents in the South China Sea, in Section 3. The results are shown in Section 4, and a discussion about what to learn from the results is in the concluding section 4.

2. Method

Harmonic analysis and complex EOFs

For each year, which needs to be defined by a twelve months period, we have 12 monthly mean values; at all spatial points x of these 12-point series, a sin-function $A(x)\ sin((t*2\pi/12) + \varphi(x))$ is fitted, with $t = 1,\ldots,12$. $A(x)$ is the amplitude, and $\varphi(x)$ is the phase. A phase $\varphi(x)=0$ indicates that the maximum of the sin-curve is in March, whereas a phase $\varphi(x)= \pi/2$ is associated with a maximum 3 months earlier, and so on.

We label the annual wave at the point x as $W(x)$. It is given either by two real numbers, the amplitude $A(x)$ and the phase $\varphi(x)$ or by one complex number $K(x) = S(x)+iC(x)$, given as $S(x)\cdot sin(t*2\pi/12) +i\ C(x)\cdot cos(k*2\pi/12)$. Both presentations are equivalent.

If we have N years, then for each year k we have one W(k,x)-annual wave, with each characterized by one of these real pairs of numbers or one complex number.

In a second step, a complex EOF analysis (von Storch and Zwiers, 1999; 16.3.2) processes the sequence of complex representations of each anomalous annual wave, i.e., of $W'(k,x) = W(k,x) - \underline{W}(x)$, with $\underline{W}(x)= \underline{A}(x)\ sin((t*2\pi/12) + \underline{\varphi}(x))$ representing the multi-year mean of all annual waves W(k,x). Thus, at each point x and each year k, we have one complex number $K(x,k) = S(x,k)+iC(x,k)$. The complex EOFs $E(x;j)$ are then the eigenvectors of the Hermitian covariance matrix $\Gamma = \langle(S+iC)^T(S-iC)\rangle$. The eigenvalues of a Hermitian matrix are real, and the eigenvectors are complex, appear in complex conjugate pairs and may thus be expressed again by two real numbers, the amplitude $a(x)$ and phase $\zeta(x)$.

The contribution of the j-th complex CEOF $E(x;j)=a(x)\ exp(i[2\pi t/12 + \zeta(x)])$ to the anomalous annual sequences W'(k,x) in year k is the product $c(k)\ E(x)$, with the complex coefficient c(k) =

Preprints (www.preprints.org) | NOT PEER-REVIEWED | Posted: 17 August 2022 doi:10.20944/preprints202208.0319.v1

$<W'(k,x)\, E^*(x)> = \gamma(k)\exp(i\,[2\pi t/12 + \delta(k)])$, with the asterisk denoting the conjugate complex pattern. This product is $c(k)\cdot E(x) = \gamma(k)\cdot a(x)\,\exp(i[2\pi t/12 + \zeta(x)+\delta(k)])$. When taking the pair of conjugate complex pairs into account, the contribution in the year k at the location x amounts to

$$M(k,x)\ \sin((t*2\pi/12 + \Delta(k,x))\ \text{ with } M(k,x) = \gamma(k)\cdot a(x) \text{ and } \Delta(k,x) = \zeta(x)+\delta(k)$$

This is the contribution of the CEOF in representing the anomalous annual wave year *k* and at data point *x*. We add this contribution to the mean field $\underline{W}(x)$ to see how this modifies the full annual wave in year k, i.e., we consider

$$\underline{A}(x)\,\sin((t*2\pi/12) + \underline{\varphi}(x)) + M(k,x)\,\sin(2\pi t/12 + \Delta(k,x))$$

$$= [\underline{A}(x)+M(k,x)\cdot\cos(\Delta'(k,x\,)]\,\sin((2\pi t/12) + \underline{\varphi}(x)\,) + [M(k,x)\,\sin(\Delta'(k,x))]\cos((2\pi t/12) + \underline{\varphi}(x)) \qquad (1)$$

with the relative phase shift $\Delta'(k,x) = \Delta(k,x) - \underline{\varphi}(x)$. According to the first term, the amplitude of the long term mean annual cycle is modified by an addition of $M(k,x)\cdot\cos(\Delta'(k,x))/A(x)$ in the year k. The second term describes a shift of the mean annual sine curve by the cosine-factor $[M(k,x)\,\sin(\Delta'(k))]\,\cos((2\pi t/12) + \underline{\varphi}(x))$. If $M(k,x) << \underline{A}(x)$ the shape of the sin-curve changes only little, same if $\sin(\Delta'(k,x))$ is small. This is the case in the example presented below.

$$W(K,x) \approx [\underline{A}(x)+M(k,x)\cdot\cos(\Delta'(k,x\,)]\,\sin((2\pi t/12) + \underline{\varphi}(x)\,) + [M(k,x)\,\sin(\Delta'(k,x))]\,\cos((2\pi t/12) + \underline{\varphi}(x))$$

$$= \mathrm{sqrt}([A(x)+M(k,x)\cdot\cos(\Delta'(k,x\,)]^{**}2+[M(k,x)\cdot\sin(\Delta'(k,x)]^{**}2)\,\sin((t*2\pi/12) + \varphi(x) + \theta(k,x))$$

with $\theta(k,x) = \tan^{-1}[M(k,x)\cdot\sin(\Delta'(k,x)]/[\underline{A}(x)+M(k,x)\cdot\cos(\Delta'(k,x\,)]$: the sin-curve of the long-year mean annual curve is shifted by $\theta(k,x)$ and the amplitude is modified by the factor $\mathrm{sqrt}\{[A(x)+M(k,x)\cdot\cos(\Delta'(k,x\,)]^2 + [M(k,x)\cdot\sin(\Delta'(k,x)]^2\}\,/A(x)$.

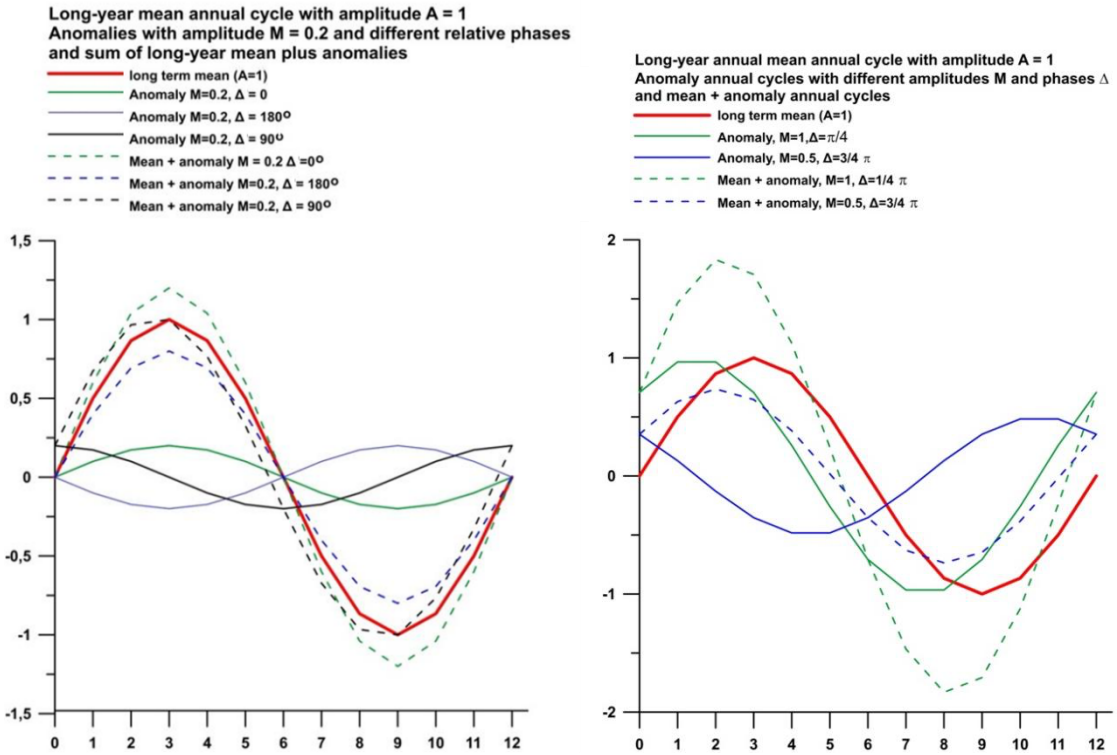

Figure 1; Synthetic example of the overlay of CEOF-estimates of dominant anomalies on the mean annual cycle. The solid red line is the long-term mean $\underline{W}$, the solid-colored lines are assumed anomalies given by CEOF 1, and the dashed lines are the overlays of mean and anomaly. Left: with a small amplitude of the anomaly, right: with a large and a moderate amplitude of the anomaly.

[3]

Preprints (www.preprints.org) | NOT PEER-REVIEWED | Posted: 17 August 2022 doi:10.20944/preprints202208.0319.v1

The effect may be illustrated by two synthetical examples, shown in Figure 1. The left diagram shows three situations, where the anomaly has a 20% amplitude of the mean, and different phases $\Delta=0$ leads to an amplification, $\Delta=180^o$ to a reduction of the amplitude, and $\Delta=90^o$ to slight shift of the mean function by something of the order in 1 month and less, without noteworthily affecting the amplitude. In the right diagram, larger anomaly amplitudes are used. When the anomaly has the same intensity as the mean, but is shifted by 45°, the sine-function is moved, with the maximum slightly shifted to the left (see the right diagram); when the anomaly amplitude is half of the mean, and the phase by 135°, the amplitude is reduced and shifted more to the left, by one or two months

3. Case: barotropic stream function

a) Region and Data used

Our test case is the barotropic flow in the South China Sea, as simulated in the STORM project (for details, refer to Zhang and von Storch (2017)). This region exhibits a marked annual cycle, which is associated with the annually reversing South-East Asian monsoon (Qian and Lee, 2000; Wang and Ding, 2008).

The 'STORM' simulation was introduced by Zhang and von Storch (2017) in this way: "The high-resolution global ocean-only simulation STORM from the German STORM consortium employed the state-of-the-art model MPI-OM and was forced by the NCEP-NCAR reanalysis data (Li and J. von Storch, 2013; Tim et al., 2015; J. von Storch et al., 2012). This simulation operates with a tri-polar grid - with a very fine grid spacing of about 0.1° and only 2.3 km at the South China Sea, and 80 unevenly distributed levels in vertical direction. The simulation was run for 6 decades of years, 1950-2010."

Several aspects of the STORM simulation data have been examined, such as the oceanic Lorenz energy cycle for the World Ocean (J. von Storch et al., 2012), the sea surface temperature (SST) near Benguela current as well as the decadal variability and trends of the upwelling system there (Tim et al., 2015). Zhang and von Storch (2017) showed that the simulation compares well with AVISO-data and the ocean reanalysis C-GLORS in terms of the annual cycle and intraseasonal variability, among others, of sea level and barotropic flow. The monsoonal variation is well reproduced, as is shown by the long term 3-month means in Figure 2 (taken from Zhang and von Storch, 2017).

As illustration, we consider the barotropic stream function in the South China Sea. We demonstrate that the results are only weakly sensitive to the choice of the 12-month segment to calculate the amplitudes and phases of the annual wave. To do so, we show in Figure 3 the mean amplitude pattern $\underline{A}$ and the mean phase pattern $\underline{\varphi}$. For the CEOF analysis, these mean fields are subtracted from all annual segments, so that the CEOFs describe changes relative to the mean maps.

These mean maps are consistent with the sequence of seasonal means, shown in Figure 2. They indicate a variation of the cyclonic flow in the South China Sea, with a cyclonic circulation, with a minimum of the streamfunction in the middle of the South China Sea, in fall and winter, while the circulation is anticyclonic in spring and summer. The maximum of the streamfunction, associated with the strongest anticyclonic circulation is in summer (Figure 3)

Preprints (www.preprints.org) | NOT PEER-REVIEWED | Posted: 17 August 2022 doi:10.20944/preprints202208.0319.v1

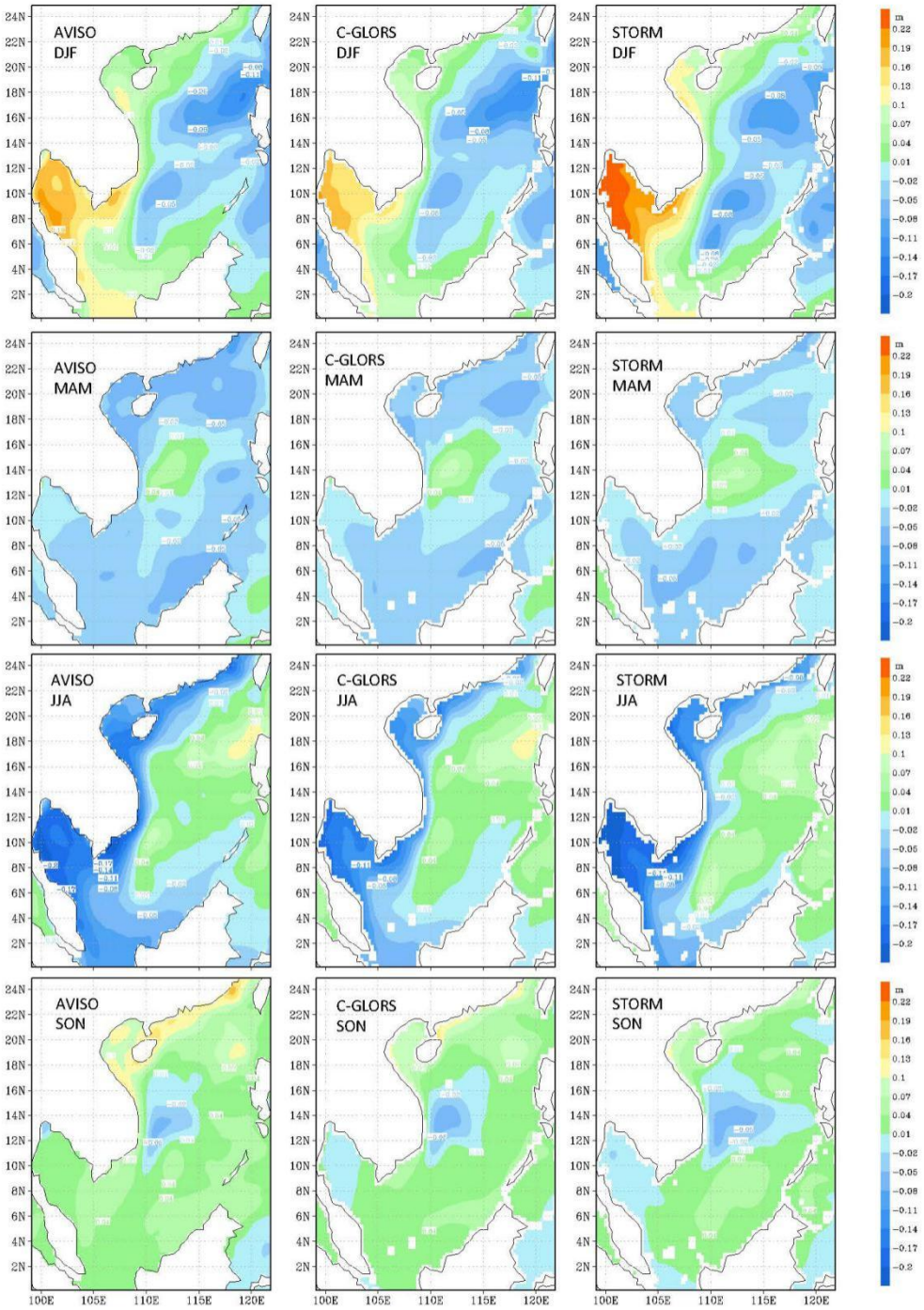

Figure 2: 1993-2010 DJF, MAM, JJA and SON means of detrended sea surface height anomalies [m] according to AVISO, C-GLORS and STORM. (From Zhang and von Storch, 2016)

Preprints (www.preprints.org) | NOT PEER-REVIEWED | Posted: 17 August 2022 doi:10.20944/preprints202208.0319.v1

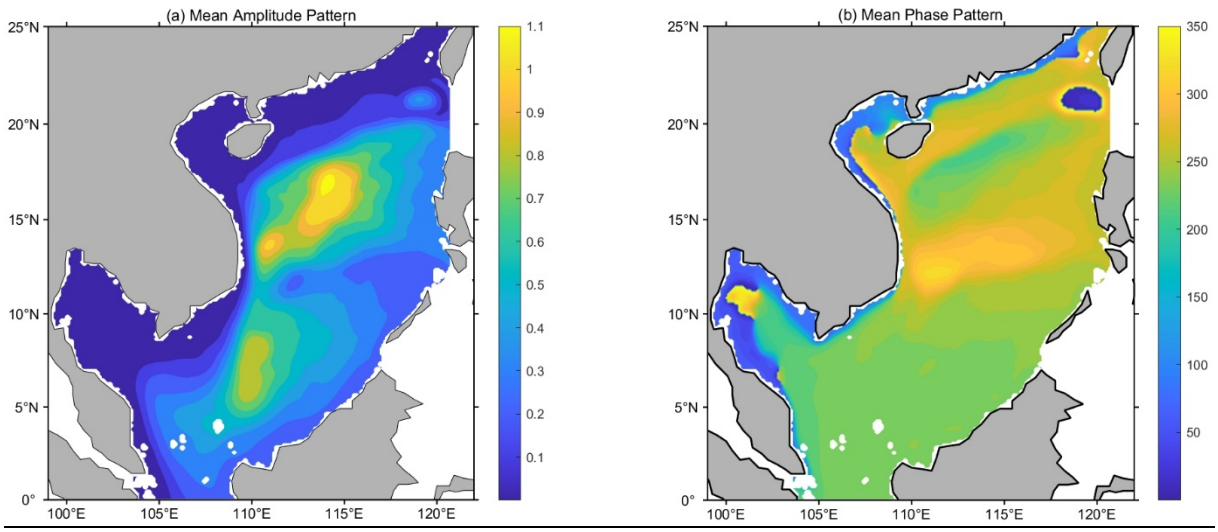

Figure 3: Long-term mean of the annual wave (derived from 61 12-monthly segments) of the barotropic stream function at all grid points of the multiyear simulation "STORM". Left: (long-term mean annual wave amplitude A; right: long-term mean phase φ, in degrees, with zero degree marking a maximum in March.

b) Results – sensitivity to the choice of annual range

To begin with, we calculate complex EOFs (CEOFs) once for January-December segments and once of July-June segments. The eigenvalue-spectra of the two analyses are shown in Figure 4 – they are virtually identical, even if the first eigenvalue, i.e., the variance represented by the first CEOF in the July-June analysis is a bit larger than the first eigenvalue of the January-December analysis.

The spectra indicate that there are at least 2 "significant eigenvalues" (Rule N of North et al., 1982), while the higher-indexed CEOFs are degenerate, i.e., may be replaced by linear combinations of these higher-indexed CEOFs. The choice of the specific patterns of the higher-indexed is to large extent random. Thus, a comparison of these in the two set-ups makes little sense, and we limit ourselves in the comparison on the first CEOFs only.

Figure 5 shows the amplitude and phase pattern and pairs of CEOF1 *E(x;1)* for the two segment-choices. The phase is set to represent in both analysis a maximum in March for a phase of zero

The patterns of the anomalous annual cycles is strongest in the center of the South China Sea, where the largest values happen in (northern) May to June. Along the coasts the annual cycle is weak with maxima a little later.

Preprints (www.preprints.org) | NOT PEER-REVIEWED | Posted: 17 August 2022 doi:10.20944/preprints202208.0319.v1

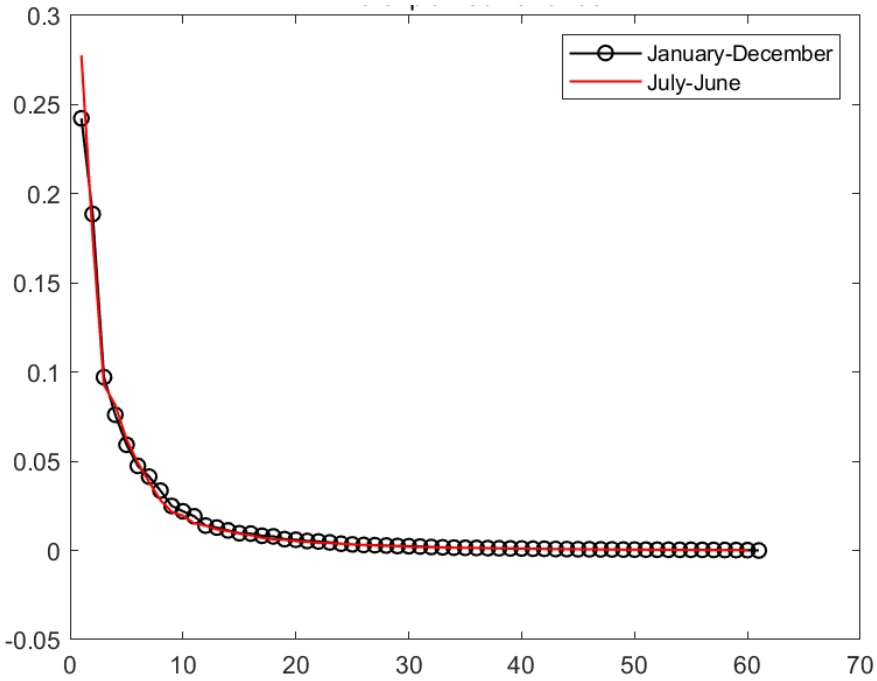

Figure 4: Spectra of eigenvalues of the CEOF analysis of annual cycles of the barotropic stream function, for two definitions of the annual window, July-June (in red) and January–December (black, with circles). Units: Proportion of variance described.

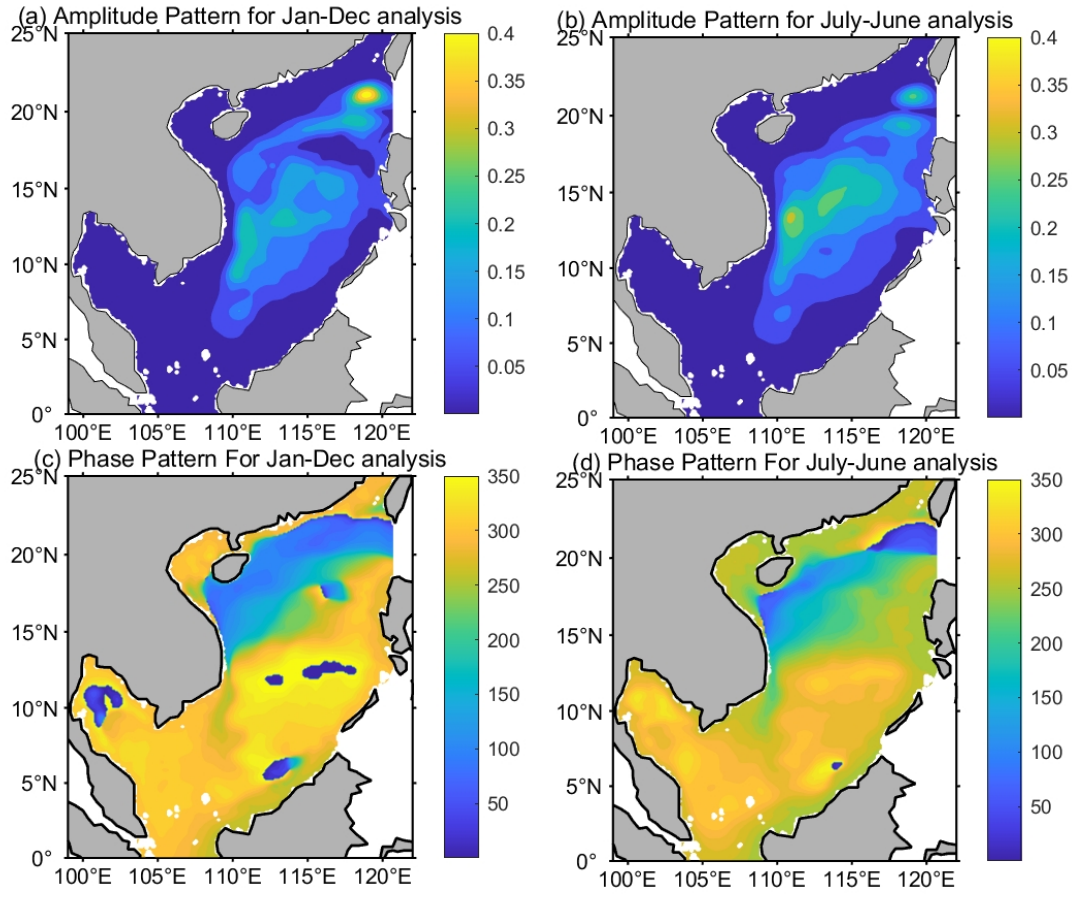

Figure 5: First CEOF patterns E(x;1), given as amplitude a and phase ζ, of the annual cycles in barotropic stream function in the South China Sea. Phase = 0 is associated with maxima in March.

Preprints (www.preprints.org) | NOT PEER-REVIEWED | Posted: 17 August 2022 doi:10.20944/preprints202208.0319.v1

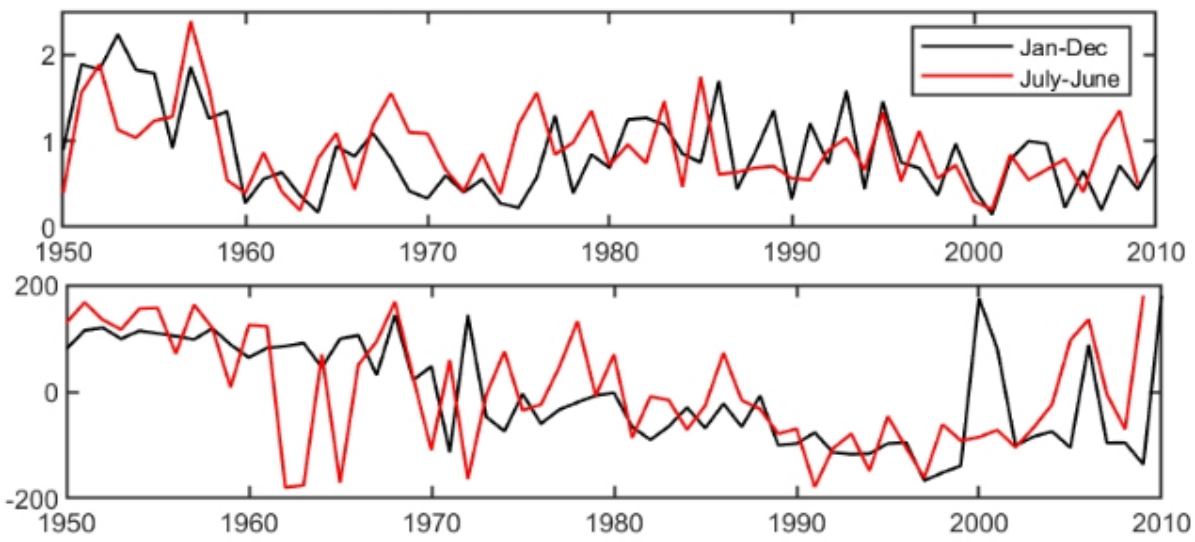

Figure 6: Time series of the principal components (coefficients) if the first CEOF of the anomalous annual cycles of the barotropic stream function. Top: amplitudes $\gamma(1)$, no units; bottom: phases $\delta(1)$, in degrees.

The two patterns are very similar, both in terms of amplitudes *a* and phases ζ. We conclude that the choice of the segments is only weakly sensitive to the choice of the segments.

The CEOF principal components c, or coefficients, in Figure 6 show quite some variability from year-to-year, so that it is not surprising that there are substantial differences in the year-to-year time scale between the two analyses, but on longer times scales, the two temporal developments are rather similar.

We conclude from these findings that we may define the segment for determining the annual cycle arbitrarily. Therefore, we chose in the following the time window from January to December.

c) Results: Analysis of the January-December analysis

In the following we consider the results only for the January-December segments, as displayed in Figures 3, 5(left) and 6 (black lines).

CEOF 1 *E(x;1)* amplitude pattern of CEOF1 (α; Figure 5, left), is similar to the mean annual cycle amplitude pattern (A; Figure 3, left): both show largest variations in the northern central part of the SCS, while in other parts, in particular in the Gulf of Thailand or along coasts the amplitudes are small.

In the center of the South China Sea CEOF1 represents roughly up to 20% of the long-term amplitude.

The CEOF is associated with a modification of the mean phase as given in Figure 3 – in the northern off-coastal strip, the phase ζ is close to zero, but in the southern central part, the phase of the anomaly can be modified by up $\pm$ 2 months (given that the phase of CEOF1 principal component is 0).

An inspection of the time series (Figure 6) suggests that the period 1950-1958 goes with a somewhat different amplitude, which may reflect the usage of the NCEP1 re-analysis to run the ocean model. Prior to 1958 the quality of NCEP1 is worse than after 1958 (Kalnay et al., 1996). In [8]

Preprints (www.preprints.org) | NOT PEER-REVIEWED | Posted: 17 August 2022 doi:10.20944/preprints202208.0319.v1

terms of the phase, there are some differences, which may appear enlarged because of passing the 360° limit.

A remarkable feature is the gradual change of the phases $\delta(k)$ of the anomalies from 1960 until about 1995, with $\delta(1960s) \sim +90^o$ to $\delta(1980/90s) \sim -90^o$. When we want to learn what this means for the full annual cycle, we add these anomalies to the time mean pattern $\underline{W}$, as given in Figure 3.

In the central South China Sea, the mean phase $\underline{\varphi}$ in Figure 3 is about 240°, corresponding to a maximum in July. The anomaly pattern in that region has a phase $\zeta \approx 240^o$ (Figure 5). When CEOF pattern *E(x;1)* is multiplied with the CEOF principal component, then the phase δ of the coefficient (Figure 6) has to be added to the phase ζ of the pattern, that is $\Delta(1960s,x) = \zeta(x)+\delta(1960s) = 240^o+90^o = 330^o$ during the 1960s, $\Delta(1970s, x) = 240^o+0^o = 240^o$, and $\Delta(1980/90s, x) = 240^o-90^o = 150^o$ during the 1980/90s.

For a grid point *x* in the central northern South China Sea, the long-term mean amplitude $\underline{A}(x)$ is about 0.8 (Figure 3). In that part of the SCS, the CEOF *E(x,1)* has an amplitude $\alpha(x)$ of only 0.2 (Figure 5). The principal component *c(1)* (Figure 6) in the 1960s as well as in the 1980/90s has an amplitude $\gamma(k,x)$ of roughly 1 (Figure 6). For the phases we have

$\Delta'(k,x) = \Delta(k,x) - \underline{\varphi}(x) =$

$= 330^o - 240^o = 90^o$ for the 1960s,

$= 240^o - 240^o = 0^o$ for the 1970s, and

$= 150^o - 240^o = -90^o$ for the 1980/90s.

and $M(k,x) = \gamma(k) \cdot a(x) = 0.2$. Thus, for a point in the central SCS we find for the *k*-th year

$$[\underline{A}(x)+M(k,x)\cdot\cos(\Delta'(k,x))]\sin((2\pi t/12) + \underline{\varphi}(x)) + M(k,x)\sin(\Delta'(k,x))\cos((2\pi t/12) + \underline{\varphi}(x))$$

- $= 0.8\sin((2\pi t/12) +240^o) + 0.2\cos((2\pi t/12) +240^o)$ in the 1960s,
- $= 1\sin((2\pi t/12) +240^o)$ in the 1970s, and

$= 0.8\sin((2\pi t/12) +240^o) - 0.2\cos((2\pi t/12) +240^o)$ in the 1980/90s

The second terms in these expressions for the 1960s and 1980/90s are relatively small, only a quarter of the mean annual cycle amplitude. From the 1960s to the 1990s, the phase of the PC moves forward in time, so that in the 1970, we have an amplitude of about 1, compared to 0.8 of the mean annual wave, but a phase close to that of the long-term mean (namely 240°).

The annual waves for three grid-points, with relatively large CEOF1 amplitudes in the South China Sea are displayed in Figure 7 for three different decades of years. **For all three points, the mean annual wave is relatively small (Figure 3).**

In the Luzon Strait, at point A, the anomalies, given by CEOF1 as solid lines, show a marked shift (black > green > blue) to earlier times – overlaid the mean, solid red curve of the mean annual waves leads to a shift (green) of the maximum from about July in the 1970s by about one month to August in the 1990s. In the 1960s (black), the annual cycle is reduced, and in the 1990s (blue) it is enhanced. From 1960s to 1970s, and from 1970s to 1990s, the amplitude of the annual cycle becomes larger and larger. However, the maximum shift from July to August, and then back to July.

At point B, in the coastal region west off Hainan, the mean annual maximum takes place later in the year than at Point A, namely at about August. The maxima of the anomalies move during the decades to earlier calendar months (black > green > blue), from August to February, which is reflected also in

Preprints (www.preprints.org) | NOT PEER-REVIEWED | Posted: 17 August 2022 doi:10.20944/preprints202208.0319.v1

the absolute annual cycles, with maxima in February in the 1990s.The amplitudes of annual cycle wave are enhanced during the decades.

Point C is located in the Central South China Sea, we find the anomalies have maxima in July, March and January, and in the mean annual wave in May. In absolute terms, the maxima move from June, over Arpil to March, and the amplitude is reduced all the time.

Thus, we find that the most important CEOF (CEOF1) describes variations of the annual cycle mostly in the phases of the annual wave, with maxima shifted by several months. At the same time, the amplitudes do not show a trend or marked interdecadal variability . Dfferent trend occur at different points.)

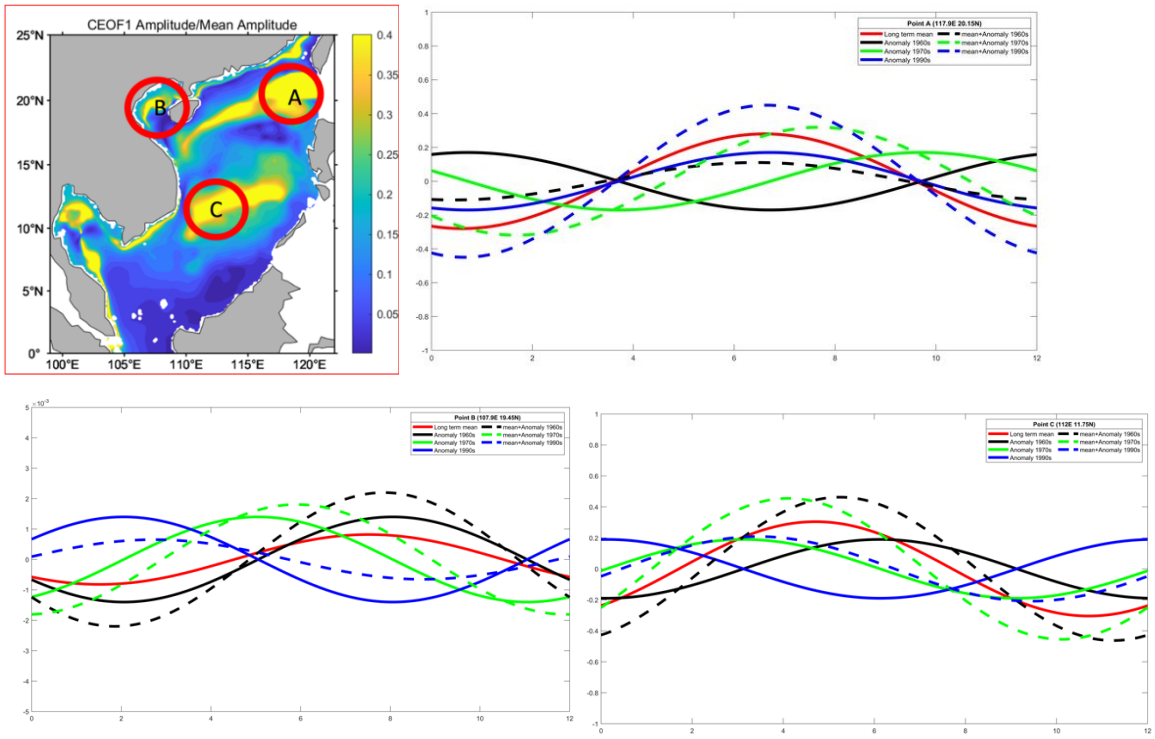

Figure 7: Change of the annual cycle from the 1960s to the 1990s at three locations, marked A, B, and C as described by CEOF1. The long-term mean annual wave W is given in red; the anomalies, represented by CEOF1 by the solid lines, and the sum of the mean and the anomaly by dashed lines. Black stands for the 1960s, green for the 1970s and blue for the 1990s
Top left: Ratio of CEOF1 amplitude $\alpha(x)$ and of long-term mean amplitude A(x), with maximum ratios in yellow and minimum in blue. The other diagrams show the CEOF anomalies, and the sum of anomaly and long-term mean – for the three points A, B, and C.-

In order to assess the influence of CEOF2 on the annual cycle we consider the annual waves at a point in the Luzon Strait (Figure 8) with relatively large CEOF2 amplitude (Figure 9). Two years with quite different amplitudes but close phases of the CEOF2 time series are chosen, namely 1992 and 2001. In both years, the anomalies, given by CEOF2 as solid lines, show a marked and similar phase shift to earlier calendar months. However, when overlaid the mean annual wave, it leads in 1992 to a shift of the maximum from about April to January, and to a doubled amplitude. On the other hand, the annual wave in 2001 is similar to the mean annual wave., with changed little changes in both phase and amplitude.

Preprints (www.preprints.org) | NOT PEER-REVIEWED | Posted: 17 August 2022 doi:10.20944/preprints202208.0319.v1

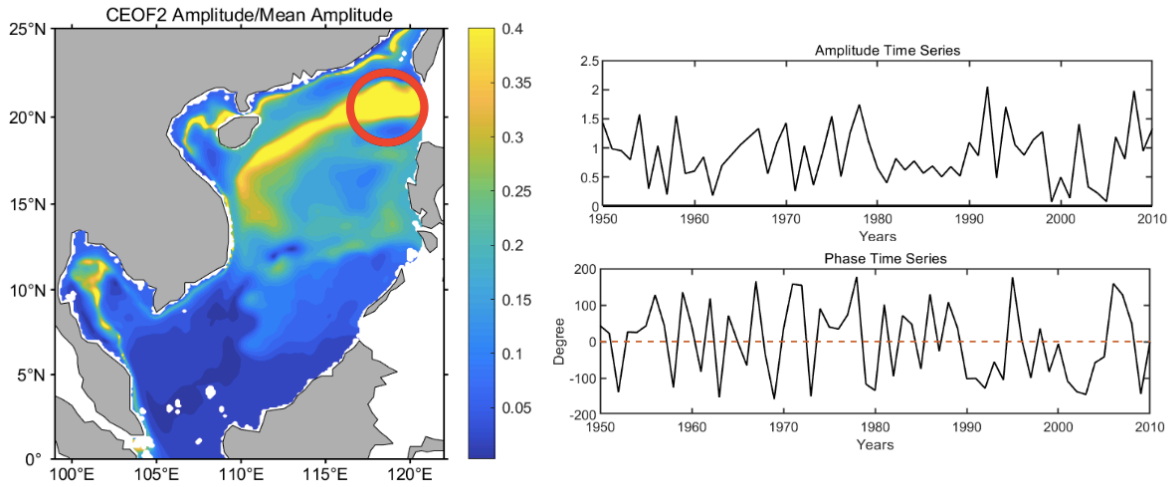

Figure 8 : Left: Ratio of CEOF2 amplitude $\alpha(x)$ and of long-term mean amplitude A(x), with maximum ratios in yellow and minimum in blue. Right: the amplitude (top) and phase (bottom) time series of CEOF2.

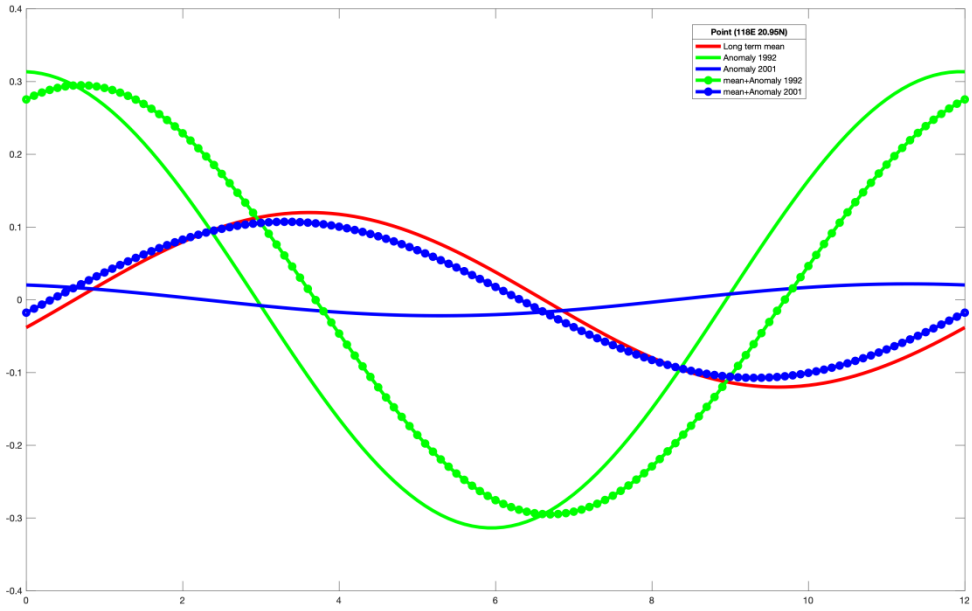

Figure 9: Change of the annual cycle in the year 1992 and the year 2001 at the location marked in Figure 8. The long-term mean annual wave W is given in red. Green stands for the year 1992 and blue for the year 2001.

4. Discussion

This article was begun to develop a method to quantify changes in the annual cycle, which is rarely considered via complex EOFs. This was achieved, but the thinking in terms of "anomalies of the annual wave" is not common, and a bit challenging, because one has to treat two variations, one of

Preprints (www.preprints.org) | NOT PEER-REVIEWED | Posted: 17 August 2022 doi:10.20944/preprints202208.0319.v1

the mean annual cycle, and another as the variations given by the COEFs. This makes the analysis less elegant than we are used from most other applications of methodology.

To demonstrate and test the method, we analyzed a data set, which was conveniently available to us, but not so much because we expected significant results on the dynamics of the ocean, or the atmosphere. We considered the barotropic stream function in the south China Sea, as simulated for several decades of years with a dynamical model.

To our surprise, we found something interesting, namely a decadal trend of the timing of the peak cyclonicity and anti-cyclonicity of the circulation in the South China Sea. When compared with the early time of the simulation, in the 1960s, the circulation cyclonicity peaks in the later part, in the 1980s and 1990s, two months earlier.

Since the gyre in the South China Sea is strongly coupled to the regional, seasonally varying monsoonal wind system, it is expected that also the forcing of the South China Sea circulation, namely mostly the monsoonal winds, change their direction also earlier than previously.

That the characteristics of monsoon system in SE Asia undergo interdecadal variations has been demonstrated by, e.g., Zeng et al. (2021), but such a trend is not documented to our knowledge. This leaves two possibilities - namely that the model-simulation, or its driving data, suffer from inhomogeneities, so that the trend may be artificial – or that we have detected a relevant trend. We will examine these options in a new study.

Another question is, what the origins of the interannual variations, as displayed in Figure 5, may be. We have examined possible links to ENSO, by comparing the COEF coefficient time series to an ENSO-index, but found only one noteworthy link, namely a link to the real part of principal component PC1, which is also reflected in the phase of that PC (Figure 10). We used the May-April mean Nino3.4 index as index of the state of ENSO. For positive ENSO-cases, i.e., El Niños, we find a trend towards increased real parts, but not for negative ENSO cases, i.e., La Niña cases, and not for the imaginary part nor the amplitude. The phase is clustering around zero, when Nino3.4 is large, but is either about 100° or -100°.

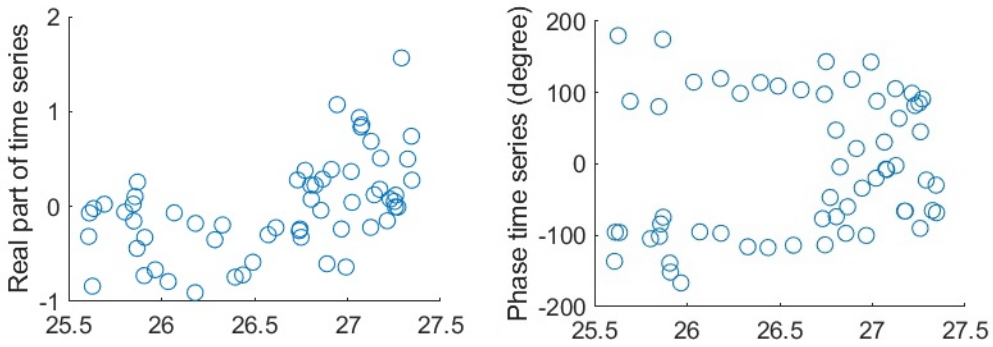

Figure 10: Scatter diagram of the real art of principal component PC1, and the phase of PC1 with the ENSO index Nino3.4 (a temperature in the central Equatorial Pacific) averaged across May to April.

Acknowledgements

We are grateful to the Max Planck Institute of Meteorology (MPI) for providing the STORM simulations. This study is supported by the National Natural Science Foundation of China (41731173 and 42192564), the National Key R&D Program of China (2019YFA0606701), the Strategic Priority Research Program of the Chinese Academy of Sciences (XDB42000000 and XDA20060502), the Key Special Project for Introduced Talents Team of Southern Marine Science and Engineering Guangdong Laboratory (Guangzhou) (GML2019ZD0306), the Innovation Academy of South China Sea Ecology and Environmental Engineering, the Chinese Academy of Sciences (ISEE2021ZD01), and the Leading Talents of Guangdong Province Program.

5. References

Deng Q., Da Nian D., and Fu, Z., 2018: The impact of inter-annual variability of annual cycle on long- term persistence of surface air temperature in long historical records, *Clim Dyn* 50:1091–1100 DOI 10.1007/s00382-017-3662-5

Dwyer, J.G., M. Biasutti, and A. H. Sobel, 2012: Projected Changes in the Seasonal Cycle of Surface Temperature. *J Climate* 25, 6359-6374. DOI: 10.1175/JCLI-D-11-00741.1

Ha, K.-J., K.Y. Heo, S.-S. Lee, K.-S. Yun, and J.-G. Jhun. 2012: Variability in the East Asian Monsoon: a review, *Meteorol. Appl.* 19: 200–215

Kalnay, E., M. Kanamitsu, R. Kistler, W. Collins, D. Deaven, L. Gandin, M. Iredell, S. Saha, G. White, J. Woollen, Y. Zhu, M. Chelliah, W. Ebisuzaki, W. Higgins, J. Janowiak, K.C. Mo, C. Ropelewski, J. Wang, A. Leetmaa, R. Reynolds, R. Jenne and D. Joseph, 1996: The NCEP/NCAR 40-Year Reanalysis Project. Bulletin of the American Meteorological Society, Vol. 77, No. 3, 437-471

Männikus, R., Soomere, T., Viška, M. 2020. Variations in the mean, seasonal and extreme water level on the Latvian coast, the eastern Baltic Sea, during 1961–2018. Estuarine, Coastal and Shelf Science, 245, art. no. 106827, doi: 10.1016/j.ecss.2020.106827.

Marcel, K., M. Biasutti, C. Binfils, K. E. Taylor, Y. Kushnir and B. Cook, 2017: Observed and Projected Changes to the Precipitation Annual Cycle. *J Climate* 30, 498-49953, DOI: 10.1175/JCLI-D-16-0572.1

North, G.R., T.L. Bell, R.F. Cahalan and F.J. Moeng, 1982: Sampling errors in the estimation of empirical orthogonal functions, Mon. Wea. Rev. 110, 699-706

Qian A, and Lee D.-K. 2000: Seasonal March of Asian summer monsoon. International Journal of Climatology. 20. 1371 - 1386. 10.1002/1097-0088(200009)20:11<1371::AID-JOC538>3.0.CO;2-V.

Stine, A.r R., P.J. Huybers, and I.Y. Fung. 2009: Changes in the phase of the annual cycle of surface temperature. *Nature* 457: 435-440.

Stine, A.R., and P. Huybers, 2012: Changes in the Seasonal Cycle of Temperature and Atmospheric Circulation. *J Climate* 25, 7362-7380

Tesouri, M., L. GImeno, R. Nieto, L. de la Torre, P, Robera, D. Gallego, R. García-Herrera, and E. Hernández,2005: Interannual variability of the annual cycle of temperature over northern Africa. *Stud. Geophys. Geod*., 49 (2005), 141_151

Thomson, D.J., 2009: Climate change: Shifts in season. *Nature*, 457, 391-392

van Loon, H., J.W. Kidson, A.B. Mullan, 1993: Decadal variation of the annual cycle in the Australian dataset. *J. Climate* 6, 1227–1231.

Vecchio, A., and V. Carbone, 2010: Amplitude-frequency fluctuations of the seasonal cycle, temperature anomalies, and long-range persistence of climate records. *Physical Rev*. E82, 066101

von Storch, H., and F. W. Zwiers, 1999: *Statistical analysis in climate research*. Cambridge University Press

Wainwright, C., J.H. Marsham, D.P. Rowell, and Emily Black, 2021: Future changes in seasonality in Eastern Africa from regional simulations with explicit and parametrised convection. XXXX, in press

Wang B., and Ding Q. 2008: Global monsoon: Dominant mode of annual variation in the tropics. Dynamics of Atmospheres and Oceans – Dynam. Atmos. Oceans. 44. 165-183. 10.1016/j.dynatmoce.2007.05.002.

Zeng Z., Guo Y., and We Z., 2021: Interdecadal Change in the Relationship Between the Bay of Bengal Summer Monsoon and South China Sea Summer Monsoon Onset. Frontiers in Earth Science. 8. 10.3389/feart.2020.610982.

张萌 (Zhang M.), and H. von Storch, 2017: Towards downscaling oceanic hydrodynamics - Suitability of a high-resolution OGCM for describing regional ocean variability in the South China Sea. *Oceanologia* 59, 166-176, DOI 10.1016/joceano.2017.01.001

张萌 (Zhang M.), H. von Storch, 王东晓 (Wang D.), 陈学恩 (Chen X.), and 李德磊 (Li D.), 2019: Statistics of travelling eddy variability in the South China Sea, 1950-2010. *Ocean Dyn.* 69: 879-898. online: https://doi.org/10.1007/s10236-019-01282-2